

# Mobility in geometrically confined membranes

Yegor A. Domanov<sup>a</sup>, Sophie Aimon<sup>a</sup>, Gilman E. S. Toombes<sup>a</sup>, Marianne Renner<sup>b</sup>, François Quemeneur<sup>a</sup>, Antoine Triller<sup>b</sup>, Matthew S. Turner<sup>c</sup>, and Patricia Bassereau<sup>a,1</sup>

<sup>a</sup>Institut Curie, Centre de Recherche, Centre National de la Recherche Scientifique, Unité Mixte de Recherche 168, Physico-Chimie Curie, Université Pierre et Marie Curie, 75248 Paris, France; <sup>b</sup>Institut de Biologie, Ecole Normale Supérieure, Institut National de la Santé et de la Recherche Médicale U1024, Centre National de la Recherche Scientifique, Unité Mixte de Recherche 8197, 75005 Paris, France; and <sup>c</sup>Department of Physics, University of Warwick, Coventry CV4 7AL, United Kingdom

Edited by Tom C. Lubensky, University of Pennsylvania, Philadelphia, PA, and approved June 16, 2011 (received for review February 17, 2011)

**Lipid and protein lateral mobility is essential for biological function. Our theoretical understanding of this mobility can be traced to the seminal work of Saffman and Delbrück, who predicted a logarithmic dependence of the protein diffusion coefficient ( $i$ ) on the inverse of the size of the protein and ( $ii$ ) on the “membrane size” for membranes of finite size [Saffman P, Delbrück M (1975) *Proc Natl Acad Sci USA* 72:3111–3113]. Although the experimental proof of the first prediction is a matter of debate, the second has not previously been thought to be experimentally accessible. Here, we construct just such a geometrically confined membrane by forming lipid bilayer nanotubes of controlled radii connected to giant liposomes. We followed the diffusion of individual molecules in the tubular membrane using single particle tracking of quantum dots coupled to lipids or voltage-gated potassium channels KvAP, while changing the membrane tube radius from approximately 250 to 10 nm. We found that both lipid and protein diffusion was slower in tubular membranes with smaller radii. The protein diffusion coefficient decreased as much as 5-fold compared to diffusion on the effectively flat membrane of the giant liposomes. Both lipid and protein diffusion data are consistent with the predictions of a hydrodynamic theory that extends the work of Saffman and Delbrück to cylindrical geometries. This study therefore provides strong experimental support for the ubiquitous Saffman–Delbrück theory and elucidates the role of membrane geometry and size in regulating lateral diffusion.**

Cell membrane fluidity is crucial for living cells. Lateral transport and mixing take molecular components from where they are delivered onto the membrane to where they are needed. Diffusion is thought to be the primary mechanism for this transport and is therefore central to a variety of fundamental biomolecular processes (1) including signaling, transport, and self-assembly (2). Whether the changes in molecular mobility alone can provide a regulatory pathway in cellular processes is one of the recurring questions in membrane biophysics. It is well established that the protein lateral mobility depends on membrane fluidity and on the size of the diffusing species and can be further modified by molecular crowding (3–5) as well as interactions with membrane microdomains (6) and the cytoskeleton (6, 7). Our aim is to study experimentally how membrane geometry and, in particular, membrane area confinement can affect the diffusion of lipids and membrane proteins. We will do this by studying tracer diffusion on membrane tubes, rather than in the more usual membrane geometry of nearly planar sheets (large-radius vesicles).

In this paper, we restrict our attention to membrane diffusion in perfectly mixed, single fluid phase membranes so as to study the role of membrane geometry on diffusion, without needing to consider additional contributions from membrane phase or molecular ordering. Although curvature of a membrane can lead to changes in membrane thickness or ordering, these effects can be neglected when the smallest radius of curvature for the surface,  $R$  (in our case the radius of the cylindrical membrane tether), is much larger than the membrane thickness,  $h$  (8). Recent theoretical work has suggested that membrane geometry should influence diffusion in a particular way (9), with the diffusion constant of tracer particles becoming smaller as the radius of a membrane

tube is reduced. The area of membrane (per unit length) in a tube should affect the local diffusion constant because the movement of any particle embedded in the membrane creates a shear gradient that is proportional to the particle velocity and inversely related to the tube size. When, for instance, the particle moves along the tube axis, the membrane on the opposite side to the particle actually flows in the opposite direction, and here  $R_{\text{tube}}$  is the relevant length over which the shear gradient extends (10). According to the fluctuation dissipation theorem (11), the larger force/velocity ratio corresponds to a smaller mobility and hence a reduced diffusion constant.

These arguments can be rigorously formalized. The first papers on the subject by Saffman and Delbrück (12, 13) are seminal. These authors analyzed the low Reynolds number hydrodynamics of an embedded disk diffusing in a quasi two-dimensional membrane. Later refinements include analyzing the effect of flows in a surrounding fluid (13, 14). Saffman and Delbrück predicted that the diffusion constant on a membrane of finite area should depend logarithmically on the ratio of the size of the membrane (frame) to the radius of the diffusant particle  $r$ . Experimental verification of this important prediction was, for many years, elusive. Very recently, experimental evidence for the logarithmic dependence on the size of the diffusant particle  $r$  has been reported (5), although some debate remains (15, 16). No possible experimental test of the corresponding logarithmic dependence on the size of the membrane frame has previously been identified. We report on just such a test in the present work. Daniels and Turner (9) have shown that for membranes in a tubular geometry, which we study here, the role of effective membrane (frame) size  $R_{\text{memb}}$  introduced by Saffman and Delbrück is played by the radius of the membrane tube  $R_{\text{tube}}$  and not, for example, by its length. More recently, Henle and Levine (10) have presented a comprehensive analysis of the membrane flows and particle mobilities in spherical and tubular membranes; their solution for longitudinal mobility in the limit of thin tubes coincides with the logarithmic dependence obtained by Daniels and Turner.

In the present work we report on measurements of tracer diffusion on membrane tubes with carefully controlled radii. These tubes were pulled from giant unilamellar vesicles (GUVs) by combining micropipette aspiration and optical trapping (17, 18). Diffusion of lipid and membrane proteins was measured by single particle tracking (SPT) of quantum dots (QDs) linked either to lipids or proteins detected with a fast and sensitive camera (19). Our primary results are that membrane geometry can significantly affect tracer diffusion and that this is consistent with a logarithmic dependence on the tube radius  $R_{\text{tube}}$ . This therefore

Author contributions: A.T., M.S.T., and P.B. designed research; Y.A.D., S.A., M.R., and F.Q. performed research; Y.A.D. and G.E.S.T. analyzed data; and Y.A.D., S.A., G.E.S.T., M.R., F.Q., A.T., M.S.T., and P.B. wrote the paper.

The authors declare no conflict of interest.

This article is a PNAS Direct Submission.

<sup>1</sup>To whom correspondence should be addressed. E-mail: patricia.bassereau@curie.fr.

This article contains supporting information online at [www.pnas.org/lookup/suppl/doi:10.1073/pnas.1102646108/-DCSupplemental](http://www.pnas.org/lookup/suppl/doi:10.1073/pnas.1102646108/-DCSupplemental).

represents experimental verification of the corresponding predictions of Saffmann and Delbrück.

## Results

Our experiments were aimed at determining how the diffusion rates of membrane components in cylindrical synthetic bilayer membrane depend upon the tube radius. We first prepared GUVs with the desired lipid and protein composition. We then used a micropipette to hold and manipulate the GUVs in the microscopy chamber (Fig. 1B). The presence of a trace amount of biotinylated lipids or proteins in the membrane provided a way to attach the GUV to streptavidin-coated polystyrene bead trapped by optical tweezers, and this bead was used to pull a thin bilayer tube away from the GUV (Fig. 1B). This experimental setup is particularly convenient (18) because it allows us to control the membrane tension  $\sigma$  while measuring the pulling force  $f$  exerted by the bead, thereby determining the radius of the tether:

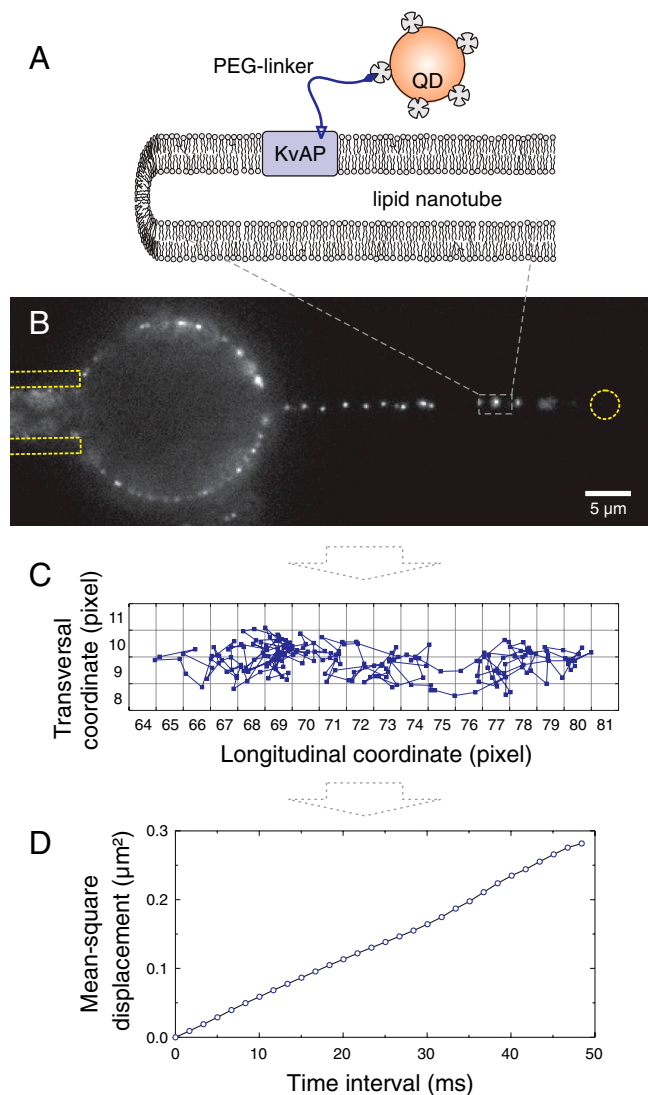


**Fig. 1.** Experimental approach to diffusion measurements on tubular membranes. (A) Schematic of the tracer molecule (KvAP in this case) embedded in the tubular membrane and labeled with QD. (B) Fluorescence of individual QD-labeled molecules diffusing on the lipid nanotube (center) and the parent vesicle (left). The nanotube is pulled using a micropipette (dotted lines on the left) holding the vesicle and an optically trapped bead (dotted circle on the right) attached at the distal tube end. (C) Example of trajectory obtained on a membrane tube. One pixel is 160 nm. (D) Averaged MSD plot for the longitudinal components of the tracer displacements obtained from multiple trajectories.

$R_{\text{tube}} = f/4\pi\sigma$  (for leaflet-symmetric, one-phase membranes). In a typical experiment, we made stepwise changes to the tube radius by changing the aspiration pressure in the micropipette and measured lateral mobility using fast SPT of streptavidin-coated QDs attached to biotinylated lipids or transmembrane proteins (Fig. 1 and Movie S1).

**Lipid Diffusion in Vesicles and Tubes.** We first analyzed a simple system consisting of a lipid tracer diffusing in a pure lipid membrane. Because of the relatively large size of the GUVs used in our experiments (radius  $>10\ \mu\text{m}$ ), we can consider the surface of the vesicle to be quasi planar and use diffusion measurements on the vesicle as a control experiment providing a reference value for a planar membrane. In the egg phosphatidylcholine (EPC) and egg phosphatidic acid (EPA) (9:1, mol/mol) membrane, we obtained  $D_{\text{planar}} = 3.3\ \mu\text{m}^2/\text{s}$  (SD =  $1.73\ \mu\text{m}^2/\text{s}$ , SEM =  $0.20\ \mu\text{m}^2/\text{s}$ , approximately 8,000 trajectories on 12 vesicles). This value is generally lower than the coefficients obtained earlier in similar systems (20, 21), which can be attributed to possible multivalent labeling of lipids in our experiments and/or the contribution from the viscous drag experienced by the QD in the aqueous phase (see below).

Next, we measured the lipid diffusion coefficients on the tubular membrane as a function of its radius (Fig. 2). We engineered sufficiently thin membrane nanotubes ( $R_{\text{tube}} = 10\text{--}250\ \text{nm}$ ) so that the whole tube could sit within the depth of field of the epifluorescence microscope. Thus, when the tube is well aligned in the focal plane, one obtains QD trajectories exploring the whole surface of the membrane tube. To avoid geometrical artefacts related to the projection of these 3D trajectories to the focal plane, we limited our analysis to the displacement components that are parallel to the tube axis (see *Materials and Methods* and ref. 22). The *Inset* in Fig. 2 shows that on wider tubes with  $R_{\text{tube}} \approx 200\ \text{nm}$ , the diffusion coefficients are scattered close to the value measured on the planar membrane (dashed horizontal line in Fig. 2 *Inset*). As we reduced the tube radius by increasing the aspiration pressure in the micropipette, the lipid mobility decreased significantly, with the most pronounced changes occurring for tube radii below 50 nm. For the thinnest tubes that we were able to obtain ( $R_{\text{tube}} \approx 10\ \text{nm}$ ) we observed more than a 3-fold reduction of the diffusion coefficient as compared to the planar membrane

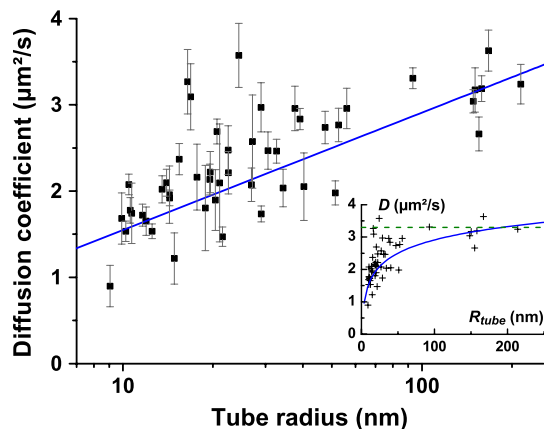


**Fig. 2.** Lipid lateral mobility on tubular membranes. Semilogarithmic plot of the diffusion coefficients calculated from longitudinal MSDs of the lipid-anchored QDs. The lipid composition was EPC/EPA (9:1, mol/mol) with additional 0.01 mol% of biotin-phosphatidylethanolamine for QD binding and tube pulling. Cumulative data from eight measurement series providing a total of 50 data points; each point represents a mean diffusion coefficient obtained from 3 to 126 individual trajectories; the error bars correspond to SEM. The weighted fit by Eq. 2 (blue solid line) yields membrane viscosity  $\eta = 5.5 \cdot 10^{-10}\ \text{J m}^{-2}\ \text{s}$  and effective lipid size  $R_{\text{lipid}} = 0.7\ \text{nm}$ . (*Inset*) The same data in linear coordinates. The mobility measured on flat membrane is shown for comparison (green dashed line;  $D_{\text{planar}} = 3.3\ \mu\text{m}^2/\text{s}$ ).

(Fig. 2). The geometrical reduction in the local membrane area (per length) in thin tubes thus appears to induce a significant reduction of lipid mobility.

Although the statistical distribution of the diffusion coefficients obtained from different trajectories in the same experiment may appear to be wide, this is typical for SPT experiments. The width of the distributions can be explained, for the most part, by stochastic variability intrinsic to the analysis of single particle trajectories rather than the lack of experimental precision. Given the SPT parameters used here (see *Materials and Methods*), the standard deviation of  $D$  predicted by statistical analysis is approximately 35% (23, 24). Some additional variation of tracer mobility, independent of the tube radius, might also result if multivalent lipid labeling occurs, in which two or more lipid molecules bind a single tracer particle (25). In our experiments, this effect would affect the lipid diffusion data more strongly than KvAP (a bacterial voltage-gated  $K^+$  channel) data, because the large size of KvAP makes it less likely that one QD could bind multiple proteins.

To ensure that there was no bias in our tracking algorithm, we systematically checked the mean-square displacement (MSD) curves and mobility histograms for all experiments. The histograms did not show large fractions of immobile particles, and the averaged longitudinal MSD curves were predominantly linear, implying Brownian diffusion in all our samples (Fig. S1). In summary, despite the relatively wide distribution of diffusion coefficients obtained by SPT, the mean values revealed a clear trend as a function of tube radius with the overall reduction of the lipid mobility significantly exceeding the experimental uncertainties.

**Transmembrane Protein Diffusion.** To understand how the tubular geometry affects mobility of a membrane component that is much larger than the size of lipid molecules, we performed SPT on a transmembrane protein reconstituted into artificial membranes. We used the KvAP, expressed in prokaryotic cells, purified following (26), and then reconstituted into GUVs using a protocol developed in our laboratory. Its close resemblance to the neuronal Kv channels (27) makes it a good model protein for studying the effect of membrane size on diffusion in structures similar in dimensions and shape to neurites and neuronal spines (28). The structure of KvAP and its conformation in the membrane are known (27), which allowed us to estimate the area occupied by the channel in the membrane and to calculate the effective radius of the tetramer to be  $R_{\text{prot}} \approx 4$  nm.

For the SPT measurements, the protein was labeled with maleimide-PEG-biotin anchor covalently attached to the protein (Fig. 1A). Protein density in the GUV membranes varied in the range of 50–1,000 proteins/ $\mu\text{m}^2$ , but only a small fraction of the total number of proteins were labeled with QDs. No biotinylated lipid was included in vesicles containing reconstituted biotinylated KvAP.

The protein diffusion coefficient on the flat membrane was  $D_{\text{planar}} = 2.3 \mu\text{m}^2/\text{s}$  (SD =  $0.7 \mu\text{m}^2/\text{s}$ , SEM =  $0.14 \mu\text{m}^2/\text{s}$ ) as calculated from a total of 3,000 trajectories on eight vesicles. This value is lower than the lipid self-diffusion coefficient given above, which is consistent with the hydrodynamic theory prediction that the lateral mobility decreases with the inclusion size.

When the KvAP diffusion was measured on tubular membranes as a function of tube radius (Fig. 3), we observed a progressive decrease of the protein lateral mobility as the tube radius was reduced, similar to the lipid-only membranes. In wider tubes ( $R_{\text{tube}} \approx 200$  nm) the lateral mobility was close to that found on planar membrane (dashed horizontal line in Fig. 3 *Inset*), but diffusion decreased rapidly in thinner ones ( $R_{\text{tube}} = 10$ –50 nm), with up to a 5-fold overall retardation of the protein diffusion in the thinnest tubes studied. This pronounced change of protein mobility in the 10- to 200-nm range of tube radii confirms our earlier conclusion that lateral mobility on narrow membrane tubes decreases as the area of membrane in the tube becomes

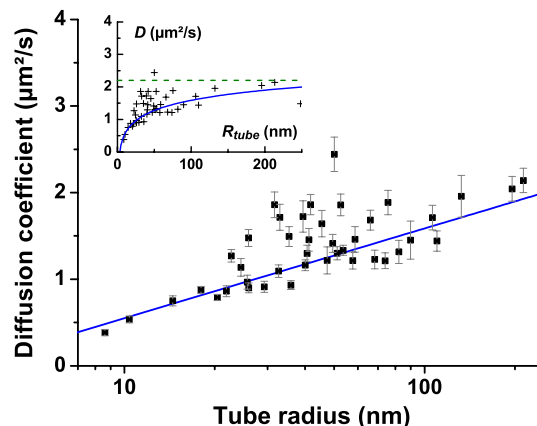


**Fig. 3.** KvAP channel mobility in membrane nanotubes. Semilogarithmic plot of longitudinal diffusion coefficient as a function of the tube radius. Protein density in the membrane varied between 50–1,000 proteins per  $\mu\text{m}^2$ . Cumulative data from seven measurement series providing a total of 43 data points; each point represents a mean diffusion coefficient obtained from 4 to 161 individual trajectories; the error bars correspond to SEM. Weighted fitting by Eq. 2 (blue solid line) yields membrane viscosity  $\eta = 7.3 \cdot 10^{-10} \text{ J m}^{-2} \text{ s}$  and protein radius  $R_{\text{prot}} = 3.0$  nm. (*Inset*) The same data in linear coordinates. The mobility measured on flat membrane is shown for comparison (green dashed line;  $D_{\text{plane}} = 2.2 \mu\text{m}^2/\text{s}$ ).

smaller. This retardation is stronger for a large transmembrane protein as compared to a lipid (Fig. 2), as expected for a hydrodynamic effect.

## Discussion

**Compatibility with Hydrodynamic Models.** Hydrodynamic models of diffusion in lipid membranes treat the bilayer as a quasi two-dimensional sheet of viscous fluid of thickness  $h$  (9, 10, 12). This is a continuum approach, and so it necessarily neglects the molecular structure and finite size of the lipids. Transmembrane proteins are modeled as cylinders of radius  $r$ , here rather larger than  $R_{\text{lipid}}$ . Because the membrane flow is effectively incompressible, the flow around a moving disk can be computed by solving Laplace's equation for a velocity potential in two dimensions (29). The mobility contains a logarithmic term, such as commonly arises in two dimensions (e.g., electrostatics). This gives rise to effects attributed to Stokes' paradox (29).

Saffman and Delbrück (12) proposed solutions for specific cases in which these logarithmic terms appear at leading order in the expression for the diffusion constant; first, for a planar membrane of finite area (e.g., on a circular frame) in a surrounding fluid of negligible viscosity:

$$D = \frac{k_B T}{4\pi\mu h} \ln \frac{R_{\text{memb}}}{r}, \quad [1]$$

where  $k_B$  is the Boltzmann constant,  $T$  is the absolute temperature,  $\mu$  is the viscosity of the membrane,  $h$  is the membrane thickness,  $R_{\text{memb}}$  is the radius of the membrane frame, and  $r$  is the radius of a disk-like tracer particle, such as a protein or lipid molecule, with  $R_{\text{memb}} \gg r$ . They then extended this to the case where the membrane has infinite area but surrounding fluid has nonvanishing viscosity  $\mu_{\text{bath}}$  (12). A new length scale emerges in the second case equal to  $\mu h / \mu_{\text{bath}}$  (12). Because of the high viscosity of the membrane, this can be of the scale of half a micron or more. It can therefore be thought of as providing a cutoff to Eq. 1: The finite membrane area appears directly unless it is larger than  $\mu h / \mu_{\text{bath}}$ , in which case the three-dimensional flows in the bulk fluid effectively screen out the logarithmic divergence arising from the purely two-dimensional membrane flow.

The concept of a planar membrane of finite area (e.g., existing on a planar frame) can seem rather artificial. Daniels and Turner (9) instead analyzed the geometry of a tubular bilayer (as well as spherical membrane geometries). They found that the diffusion constant for tracers on a membrane tube is given by an equation identical to Eq. 1, except that  $R_{\text{memb}}$  is replaced by  $R_{\text{tube}}$ , which then plays the role of the effective membrane size:

$$D = \frac{k_B T}{4\pi\mu h} \left( \ln \frac{R_{\text{tube}}}{r} \right). \quad [2]$$

Importantly, the length scale  $\mu h / \mu_{\text{bath}} \gg R_{\text{tube}}$  for all of the experimental data we present here. This means that flows in the embedding fluid can be safely neglected throughout and that we expect the diffusion constant to be given by Eq. 2.

We first compared this hydrodynamic model to our measurements of lipid diffusion (Fig. 2). We applied the Saffman–Delbrück model (12) to  $D_{\text{planar}} = 3.3 \mu\text{m}^2/\text{s}$  obtained on GUVs assuming  $\mu_{\text{bath}} = 1.25 \times 10^{-3} \text{ Pa}\cdot\text{s}$  and  $r = R_{\text{lipid}} = 0.5 \text{ nm}$  (30). We thus arrive at a 2D membrane viscosity  $\eta \equiv \mu h = 6.5 \times 10^{-10} \text{ J m}^{-2} \text{ s}$  [divided by  $h = 4.5 \text{ nm}$  (30), it gives 3D viscosity  $\mu = 1.4 \text{ P}$  (poise) or  $0.14 \text{ Pa}\cdot\text{s}$ ], which agrees well with the literature data for similar lipid compositions (31). We then fitted data for the diffusion constant of lipid tracers on a tube using Eq. 2. During the fitting procedure, the data points (points in Fig. 2) were assigned weights inversely proportional to the variance for each averaged value of  $D$  in order to account for differences in the experimental distributions of  $D$ . The logarithmic theoretical prediction (solid line in Fig. 2) closely follows the data points. Using both  $\eta$  and  $R_{\text{lipid}}$  as adjustable parameters in the fit, we obtained  $\eta = (5.5 \pm 0.8) \times 10^{-10} \text{ J m}^{-2} \text{ s}$  (equivalent to  $1.2 \text{ P}$  or  $0.12 \text{ Pa}\cdot\text{s}$ ) and  $R_{\text{lipid}} = 0.73 \pm 0.36 \text{ nm}$ ; i.e., membrane viscosity similar to the value calculated for the planar membrane above and the lipid size that is very close to the expected value (30). Similarly, if we fixed  $R_{\text{lipid}}$  at  $0.5 \text{ nm}$  and adjusted the viscosity only, we would obtain  $\eta = 6.1 \times 10^{-10} \text{ J m}^{-2} \text{ s}$ ; i.e., the fitting parameters are well defined and consistent irrespective of the fitting procedure. Remarkably, the measurements are directly compatible with this simple physical model, using literature values of  $R_{\text{lipid}}$  and  $\eta$ , with no need for any empirical/artificial adjustable parameters. This is the first confirmation that Eq. 2 is consistent with our data on lateral diffusion on the tubular membrane.

Additionally, the lipid diffusion constants on planar and tubular membranes are mutually consistent: The lipid mobility on the thickest tubes convincingly approaches that measured on almost planar membranes (Fig. 2 *Inset*). As a result, the measurements are consistent with both the Saffman–Delbrück model for planar membranes (12) and the Daniels–Turner model for tubes with very similar membrane viscosities (Eq. 2).

Moreover, our lipid diffusion data seem to agree rather well with the continuous hydrodynamic models, even though the size of the diffusing species in this case is comparable to the size of the “solvent” (lipid) particles. Strictly speaking, this represents the edge of the regime of universal validity of such continuum theories (31, 32). The diffusion of large transmembrane proteins, such as KvAP used here, is more clearly in the hydrodynamic regime. Assuming that the effective radius of KvAP in the membrane is  $R_{\text{prot}} = 4 \text{ nm}$  (27) we can then use the Saffman–Delbrück model (Eq. 1) to relate the  $D_{\text{planar}}$  value of KvAP, measured on the GUV surface, to obtain the 2D membrane viscosity  $\eta = 6.7 \times 10^{-10} \text{ J m}^{-2} \text{ s}$ . It is most reassuring that this value is close to the viscosity extracted from the diffusion of lipid tracers in lipid-only membranes, estimated above.

For the KvAP proteins, we also obtained a good fit of the tube diffusion data (Fig. 3) by the predicted logarithmic dependence (Eq. 2) with  $\eta = (7.3 \pm 0.5) \times 10^{-10} \text{ J m}^{-2} \text{ s}$  and  $r = 3.0 \pm 0.5 \text{ nm}$ . As in the case of lipid diffusion, the data appear to be consistent with the theoretically predicted logarithmic relationship (solid

line in Fig. 3). Fig. 3 presents the data and the theoretical curve in semilogarithmic coordinates to emphasize the logarithmic relationship between the protein mobility and the size of the tubular membrane. The membrane viscosity deduced from this dependence is in good agreement with the estimate calculated from the protein diffusion on flat membranes as well as our earlier estimates for pure lipid membranes. Moreover, the estimate of  $r$  is close to the value  $R_{\text{prot}} = 4 \text{ nm}$  derived from the KvAP structure (27). This is the second confirmation that Eq. 2 is valid and that hydrodynamic models correctly describe lateral diffusion in confined membranes.

**Other Possible Factors Affecting the Data.** In this paper, we show that hydrodynamic effects in tubular membranes with small radii can lead to changes of the mobility of membrane components. Several other effects can potentially affect diffusion in our system. We consider them in detail in this subsection.

The QDs used here to trace the movements of membrane components are relatively large, and hence the viscous drag experienced by the QD itself as it moves through the aqueous solvent might affect the overall mobility measured in our experiments. Assuming that the radius of QD625 is  $R_{\text{QD}} = 10 \text{ nm}$ , we calculated the 3D diffusion coefficient of the QD using Stokes–Einstein equation. For room temperature and the buffer viscosity of  $1.2510^{-3} \text{ Pa}\cdot\text{s}$ , the diffusion coefficient is  $19.6 \mu\text{m}^2/\text{s}$ , which is more than five times faster than the lipid or protein diffusion coefficients reported above. This means that the viscous drag on the tethered QD is dominated by the drag on the anchor (lipid or protein) moving through the membrane. The contribution of the nonnegligible drag on the QD can be approximated by adding the QD friction coefficient in the numerator of Eq. 2 and using this modified equation to fit the diffusion data. Following this procedure, we obtained equally good fit (or even slightly better for the lipid diffusion data) and parameters very close to those before the correction:  $\eta = 4.5 \times 10^{-10} \text{ J m}^{-2} \text{ s}$  and  $r = 0.84 \text{ nm}$  for the lipid diffusion, and  $\eta = 6.3 \times 10^{-10} \text{ J m}^{-2} \text{ s}$  and  $r = 3.4 \text{ nm}$  for the protein diffusion. Therefore, this effect does not affect our conclusions about the dependence of mobility on the tube radius; the addition of the QD friction only results in a slight vertical shift of the whole curve in Figs. 2 and 3. Although the relatively large QDs are outside the membrane tube, both KvAP and PEG lipids in the inner leaflet protrude into the inside of the membrane tube. However, these should not act as steric obstructions to diffusion because the estimated size of these protrusions (2–5 nm) is considerably smaller than the internal diameter of even the smallest tubes (13 nm).

In these experiments, changes in tube radius were accompanied by changes in membrane tension and curvature. Could membrane tension or curvature directly affect diffusion coefficients? The free area theory predicts that the diffusion coefficient should increase when the membrane is stretched to effectively increase the area of “voids” between lipids (32). In a control experiment, we have measured  $D$  on the surface of GUVs for different membrane tensions in the range of  $10^{-6}$ – $10^{-4} \text{ N/m}$ , covering the range of values used in our tube experiments (Fig. S2). We found no statistically significant change of  $D$ , confirming that the effects that we measure in our tube experiments are only related to the tube radius and not to the membrane tension. Much higher tensions ( $\sigma > \text{a few } 10^{-4} \text{ N/m}$ ) corresponding to the “stretching regime” (33) might be necessary for a noticeable effect on the diffusion. Although NMR measurements of acyl chain dynamics revealed only limited effects for even the largest membrane curvatures used in this study (34), it is important to consider how membrane curvature could alter membrane structure and dynamics. In our experimental measurements of lipid diffusion, we selectively label the lipids in the outer leaflet. The positive curvature of the outer leaflet is expected to decrease the lateral packing density at the head-group level (35). Provided that mem-

brane viscosity is determined mainly by interactions at this level (36), increased curvature would speed up diffusion in the outer leaflet. Thus, if tube curvature significantly affected lipid diffusion, one would expect faster diffusion in tubes with smaller radii, which is contrary to our observations. Furthermore, membrane curvature should affect lipids in the outer leaflet and a transmembrane object such as KvAP differently, yet both follow the logarithmic dependence predicted by Saffman–Delbrück. In summary, for this range of membrane curvatures, there is no clear evidence for a direct effect of membrane curvature on diffusion coefficients.

We also remark on the role of interleaflet flows. These have been shown to result in significant dynamical effects in cases when the membrane geometry is changing (37, 38), particularly during tube extension (38). It is important to note that our system is rather different in that the geometry is fixed and our tube is assumed to be fully equilibrated. The role of interleaflet friction in our system can be analyzed by writing down separate Stokes equations for the two leaflets that include an interlayer coupling, which is simply proportional to the velocity difference across the two leaflets but which, by Newton's third law, has a different sign on each leaflet. Importantly, these two equations can be added together to obtain an equation for the mean flow, which has the form assumed here, and used in refs. 9, 12, and 14, up to corrections that are quadratically small in the ratio of the leaflet thickness to the tube radius (i.e., a few percent). Changes in the average membrane viscosity, associated with changes in molecular ordering, could enter at the same order. A detailed analysis of these corrections is beyond the scope of the present work.

Finally, molecular crowding in the membrane can slow down the dynamics of the membrane components. At high protein densities, both protein and lipid mobility decrease because of steric hindrances imposed by large molecules. This has been predicted theoretically (39) and shown experimentally both in model membranes (3) and live cells (4). Recent data for three integral proteins with  $R_{\text{prot}} = 2\text{--}4$  nm (5) suggest that this effect becomes noticeable when the protein density exceeds around 1,000 proteins/ $\mu\text{m}^2$ . The densities of KvAP in our experiments were in the range of 50–1,000 proteins/ $\mu\text{m}^2$ ; i.e., most of our measurements fall in the safe range. Even if the crowding effects are not negligible, they will not compromise our conclusions because they will affect diffusion rates in tubes of different radii to the same degree. However, if the high membrane curvature affects the protein redistribution between the GUV and the tube causing relative enrichment of protein in thin tubes, the crowding effects can be selectively amplified for small tube radii. The study of such curvature-induced protein sorting in thin tubes is currently underway in our laboratory. Nevertheless, the mutual consistency between lipid and protein diffusion constants implies that the principal source of the mobility changes is hydrodynamic in origin and is not related to protein crowding.

In conclusion, the observed diffusion of a lipid and a transmembrane protein in tubular membranes are both consistent with the effect of confinement on the Saffman–Delbrück model. Although the role of other effects cannot be completely excluded and other mathematical functions, different from a logarithmic dependence, could be used to fit the data, these results provide strong support for the use of hydrodynamic models to describe lateral diffusion in confined membranes.

**Role in Cellular Processes.** As described above, our experimental results represent a direct test of predictions of the hydrodynamic theory for geometrically confined membranes, thus contributing to the important debate on biophysical modeling of membrane dynamics. At the same time, these findings can provide insight into a possible regulatory role of bilayer geometry in various cellular contexts. Indeed, the problem is relevant to a number of physiological processes taking place in tubular membranes such

as cell–cell communication via tunneling nanotubes (22), mobility and redistribution of membrane components in endoplasmic reticulum and Golgi apparatus (40), or receptor diffusion in neurites and neuronal spines (28, 41). The spines, representing thin protrusions on dendrite membrane that form synaptic connections to other neurones, are particularly interesting because they have tubular necks with radii in the range of 25–250 nm, and the changes of their morphology are known to correlate with synaptic plasticity (42). Fluorescence recovery after photobleaching measurements in live neurones have shown that the diffusion is slower in the spine neck region (28). At the same time, it is well known that many receptors in cytoplasmic membranes have intracellular domains that interact with the underlying cytoskeletal structure; in such cases, the drag with the cytoskeleton can decrease diffusion rates by orders of magnitude and effectively mask the more subtle hydrodynamic effects (43).

To test whether the membrane confinement effects can manifest themselves in intact biological membranes, we reproduced our SPT measurements on neurites of live hippocampal neurons in culture. We used three tracer molecules with different sizes of the transmembrane segment and obtained their diffusion coefficients as a function of the neurite width (Fig. S3). Not surprisingly, the experimental data were even more scattered than those for the model nanotubes (Figs. 2 and 3) because of possible inhomogeneities in the neurite membrane, deviations from tubular shape, interactions with cytoskeleton, dimerization/oligomerization, etc. Nevertheless, in all three cases we observed reduction of the mobility in thinner neurites that was similar to that found for model membrane tubes. Fitting these data with a simple hydrodynamic model (Eq. 2) did not yield expected sizes of the tracers (Table S1), reflecting the complex nature of the neurite biomembranes. However, the inverse dependence of the protein mobility on the neurite diameter suggests that hydrodynamic interactions in geometrically confined membranes may affect the diffusion of membrane components in living cells.

To conclude, our data suggest that membrane morphology may have a direct effect on the lateral mobility of membrane proteins in living systems and could be involved in regulatory circuitry of the cell.

## Materials and Methods

**Preparation of Lipid Vesicles, QD Labeling, and Pulling Nanotubes.** GUVs were prepared by electroformation on indium-tin oxide coated glass slides (44) using a mixture of chicken EPC and chicken EPA in a 9:1 molar ratio, complemented with 0.01% of 1,2-distearoyl-sn-glycero-3-phosphoethanolamine-N-[biotinyl(polyethylene-glycol)-2000] [DSPE-PEG(2000)-biotin]. The vesicles were in a sucrose solution with an osmolarity of 200 mOsm. Prior to the SPT experiments, the GUV suspension was diluted with a buffer solution of matching osmolarity containing approximately 10 pmol of QD625-streptavidin conjugate. After 1–2 min of incubation, the vesicles were washed with the same buffer solution using a minicentrifuge. QD-labeled GUVs were transferred to the microscopy observation chamber pretreated with casein solution and aspirated in a glass micropipette using a micromanipulator and a custom-made hydraulic system. The bilayer tube (tether) was pulled by pushing the GUV against a streptavidin-coated polystyrene bead ( $\phi = 3.3$   $\mu\text{m}$ ) held with a custom-made fixed optical trap (18) and then gently moving the vesicle away from the bead.

**Purification and Reconstitution of KvAP.** KvAP was purified and labeled using a protocol modified from ref. 26. The wild-type KvAP plasmid was generously provided by R. MacKinnon (The Rockefeller University, New York). KvAP was expressed in *Escherichia coli* solubilized in decylmaltopyranoside (DM; Affymetrix) and then purified using a His-tag affinity nickel column followed by size exclusion chromatography. The protein was labeled for 2 to 4 h at room temperature in 600  $\mu\text{M}$  of EZ-Link maleimide-PEO11-biotin (Pierce). The labeled protein was then mixed with small unilamellar vesicles (SUVs) of EPC:EPA (9:1 molar ratio) presolubilized with DM. The free label and detergent were removed by dialysis. GUVs were made using an electroformation protocol adapted from ref. 45. SUVs containing proteins were mixed with pure EPC/EPA SUVs to achieve a final lipid/protein weight ratio between 8 and 200. Droplets of the SUV mixture (3 to 10 mg/mL of lipid) were spread

on platinum wires and partially dehydrated for typically 20 min. Lipid-protein films were rehydrated in a solution containing 200 mM sucrose, 100 mM KCl, 10 mM Hepes, pH = 7.4, while keeping the platinum wires under sinusoidal voltage of 1.8 V (peak-to-peak) at 500 Hz for 4 to 12 h. The resulting GUVs were then labeled with QDs using the protocol described in the previous subsection.

**QD Imaging and Analysis.** The high-speed imaging of single QDs attached to tracer molecules was made using an epifluorescence microscope equipped with back-thinned electron-multiplying CCD camera (iXon DU-897, Andor Technology). For each tube, at a given diameter a sequence of 1,000 or 2,000 images was obtained with 1- or 4-ms exposure time and electron multiplication gain of 200. In a typical experiment, we would have between 2–10 individual QDs on a membrane tube of 20–50  $\mu\text{m}$  in length. Tracking of individual QDs was performed with the MATLAB software developed in the group of Maxime Dahan at the École Normale Supérieure (Paris, France), with modifications. Only the trajectories that were at least 30 points long were kept for further analysis. For the calculation of diffusion coefficients on the tubular membranes, we rotated the coordinate plane to precisely align the tube axis with the  $x$  axis of the coordinate plan and we only used the longitudinal (along the  $x$  axis) displacements of the particles to calculate the MSD to avoid geometrical artifacts due to curved geometry (22). The diffu-

sion coefficient  $D$  was calculated by fitting the points 2 to 5 of the MSD plot versus time with  $\text{MSD}(t) = 2Dt + b$ , where  $b$  is the variable offset used to account for limited localization accuracy (46). For each tube radius, we typically obtained 20–100 trajectories. The MSD and  $D$  were calculated for each trajectory and then averaged. For the trajectories obtained on the GUV surface, both  $x$  and  $y$  displacements were analyzed. In this case, the MSD and diffusion coefficients were calculated using conventional formulas for two dimensions.

**ACKNOWLEDGMENTS.** P.B. and Y.A.D. thank S. Morlot and A. Roux for the use of their microscope setup, B. Sorre for initial experimental tests, M. Dahan (Ecole Normale Supérieure) for expert advice, and J.-F. Joanny for stimulating discussions and carefully reading the manuscript. The project was funded by the Agence Nationale de la Recherche, Grants Neur-043-02 and BLAN-0282-02. Y.D. was supported by a fellowship from the Fondation Pierre-Gilles de Gennes and by a European Reintegration Grant from the European Commission (Marie Curie Actions). S.A. thanks D. Schmidt and R. MacKinnon (Rockefeller) for help with protein purification. G.E.S.T. was supported by a Marie Curie Incoming International Fellowship from the European Commission. M.S.T. thanks the Gulliver lab and Pierre Sens at Ecole Supérieure de Physique et de Chimie Industrielles (ESPCI) Paris for a Joliot-Curie visiting fellowship and the UK ESPI for a Leadership Fellowship, Grant EP/E501311/1. P.B.'s group belongs to the French research consortium "CellTiss."

- Axelrod D (1983) Lateral motion of membrane proteins and biological function. *J Membr Biol* 75:1–10.
- Alberts B, et al. (2002) *Molecular Cell Biology of the Cell* (Garland Science, New York), 4th Ed.
- Peters R, Cherry RJ (1982) Lateral and rotational diffusion of bacteriorhodopsin in lipid bilayers: Experimental test of the Saffman–Delbrück equations. *Proc Natl Acad Sci USA* 79:4317–4321.
- Frick M, Schmidt K, Nichols BJ (2007) Modulation of lateral diffusion in the plasma membrane by protein density. *Curr Biol* 17:462–467.
- Ramadurai S, et al. (2009) Lateral diffusion of membrane proteins. *J Am Chem Soc* 131:12650–12656.
- Lenne PF, et al. (2006) Dynamic molecular confinement in the plasma membrane by microdomains and the cytoskeleton meshwork. *EMBO J* 25:3245–3256.
- Kusumi A, Sako Y, Yamamoto M (1993) Confined lateral diffusion of membrane receptors as studied by single particle tracking (nanovid microscopy). Effects of calcium-induced differentiation in cultured epithelial cells. *Biophys J* 65:2021–2040.
- Safran SA (2003) *Statistical Thermodynamics of Surfaces, Interfaces, and Membranes* (Westview Press, Boulder, CO).
- Daniels DR, Turner MS (2007) Diffusion on membrane tubes: A highly discriminatory test of the Saffman–Delbrück theory. *Langmuir* 23:6667–6670.
- Henle ML, Levine AJ (2010) Hydrodynamics in curved membranes: The effect of geometry on particulate mobility. *Phys Rev E Stat Nonlin Soft Matter Phys* 81:011905.
- Einstein A (1905) Über die von der molekularkinetischen theorie der wärme geforderte bewegung von in ruhenden flüssigkeiten suspendierten teilchen [On the movement of small particles suspended in a stationary liquid demanded by the molecular-kinetic theory of heat]. *Ann Phys* 322:549–560.
- Saffman PG, Delbrück M (1975) Brownian motion in biological membranes. *Proc Natl Acad Sci USA* 72:3111–3113.
- Saffman PG (1976) Brownian motion in thin sheets of viscous fluid. *J Fluid Mech* 73:593–602.
- Stone HA, Ajdari A (1998) Hydrodynamics of particles embedded in a flat surfactant layer overlying a subphase of finite depth. *J Fluid Mech* 369:151–173.
- Gambin Y, et al. (2006) Lateral mobility of proteins in liquid membranes revisited. *Proc Natl Acad Sci USA* 103:2098–2102.
- Naji A, Levine AJ, Pincus PA (2007) Corrections to the Saffman–Delbrück mobility for membrane bound proteins. *Biophys J* 93:L49–L51.
- Hochmuth RM, Wiles HC, Evans EA, McCown JT (1982) Extensional flow of erythrocyte membrane from cell body to elastic tether. II. Experiment. *Biophys J* 39:83–89.
- Sorre B, et al. (2009) Curvature-driven lipid sorting needs proximity to a demixing point and is aided by proteins. *Proc Natl Acad Sci USA* 106:5622–5626.
- Dahan M, et al. (2003) Diffusion dynamics of glycine receptors revealed by single-quantum dot tracking. *Science* 302:442–445.
- Doeven MK, et al. (2005) Distribution, lateral mobility and function of membrane proteins incorporated into giant unilamellar vesicles. *Biophys J* 88:1134–1142.
- Przybylo M, et al. (2006) Lipid diffusion in giant unilamellar vesicles is more than 2 times faster than in supported phospholipid bilayers under identical conditions. *Langmuir* 22:9096–9099.
- Wieser S, Schutz GJ, Cooper ME, Stockinger H (2007) Single molecule diffusion analysis on cellular nanotubules: Implications on plasma membrane structure below the diffraction limit. *Appl Phys Lett* 91:233901–233903.
- Saxton MJ (1997) Single-particle tracking: The distribution of diffusion coefficients. *Biophys J* 72:1744–1753.
- Qian H, Sheetz MP, Elson EL (1991) Single particle tracking. Analysis of diffusion and flow in two-dimensional systems. *Biophys J* 60:910–921.
- Lee GM, Ishihara A, Jacobson KA (1991) Direct observation of brownian motion of lipids in a membrane. *Proc Natl Acad Sci USA* 88:6274–6278.
- Ruta V, Chen J, MacKinnon R (2005) Calibrated measurement of gating-charge arginine displacement in the KvAP voltage-dependent  $\text{K}^+$  channel. *Cell* 123:463–475.
- Lee SY, Lee A, Chen J, MacKinnon R (2005) Structure of the KvAP voltage-dependent  $\text{K}^+$  channel and its dependence on the lipid membrane. *Proc Natl Acad Sci USA* 102:15441–15446.
- Ashby MC, Maier SR, Nishimune A, Henley JM (2006) Lateral diffusion drives constitutive exchange of AMPA receptors at dendritic spines and is regulated by spine morphology. *J Neurosci* 26:7046–7055.
- Lamb H (1997) *Hydrodynamics* (Cambridge Univ Press, New York).
- Nagle JF, Tristram-Nagle S (2000) Structure of lipid bilayers. *Biochim Biophys Acta* 1469:159–195.
- Vaz WLC, Goodsaid-Zalduendo F, Jacobson K (1984) Lateral diffusion of lipids and proteins in bilayer membranes. *FEBS Lett* 174:199–207.
- Almeida PFF, Vaz WLC (1995) Lateral diffusion in membranes. *Structure and Dynamics of Membranes—From Cells to Vesicles (Handbook of Biological Physics)*, eds R Lipowsky and E Sackmann (Elsevier, Amsterdam), Vol 1, pp 305–357.
- Evans E, Rawicz W (1990) Entropy-driven tension and bending elasticity in condensed-fluid membranes. *Phys Rev Lett* 64:2094–2097.
- Lepore LS, Ellena JF, Cafiso DS (1992) Comparison of the lipid acyl chain dynamics between small and large unilamellar vesicles. *Biophys J* 61:767–775.
- Risselada HJ, Marrink SJ (2009) Curvature effects on lipid packing and dynamics in liposomes revealed by coarse grained molecular dynamics simulations. *Phys Chem Chem Phys* 11:2056–2067.
- Venable RM, Zhang YH, Hardy BJ, Pastor RW (1993) Molecular-dynamics simulations of a lipid bilayer and of hexadecane—An investigation of membrane fluidity. *Science* 262:223–226.
- Yeung A, Evans E (1995) Unexpected dynamics in shape fluctuations of bilayer vesicles. *J Phys II* 5:1501–1523.
- Evans E, Yeung A (1994) Hidden dynamics in rapid changes of bilayer shape. *Chem Phys Lipids* 73:39–56.
- Abney JR, Scalettar BA, Owicki JC (1989) Self diffusion of interacting membrane proteins. *Biophys J* 55:817–833.
- Polishchuk RS, Capestrano M, Polishchuk EV (2009) Shaping tubular carriers for intracellular membrane transport. *FEBS Lett* 583:3847–3856.
- Renner M, Choquet D, Triller A (2009) Control of the postsynaptic membrane viscosity. *J Neurosci* 29:2926–2937.
- Yuste R, Bonhoeffer T (2001) Morphological changes in dendritic spines associated with long-term synaptic plasticity. *Annu Rev Neurosci* 24:1071–1089.
- Evans E, Sackmann E (1988) Translational and rotational drag coefficients for a disk moving in a liquid membrane-associated with a rigid substrate. *J Fluid Mech* 194:553–561.
- Angelova MI, Soléau S, Méléard P, Faucon JF, Bothorel P (1992) Preparation of giant vesicles by external AC electric fields. Kinetics and applications. *Prog Colloid Polym Sci* 89:127–131.
- Méléard P, Bagatolli LA, Pott T (2009) Giant unilamellar vesicle electroformation: From lipid mixtures to native membranes under physiological conditions. *Methods in Enzymology*, ed D Nejat (Academic, London), Vol 465, pp 161–176.
- Savin T, Doyle PS (2005) Static and dynamic errors in particle tracking microrheology. *Biophys J* 88:623–638.